JACS
JOURNAL OF THE AMERICAN CHEMICAL SOCIETY

Article

pubs.acs.org/JACS

Meso-Structured Platinum Thin Films: Active and Stable Electrocatalysts for the Oxygen Reduction Reaction

Jakob Kibsgaard, Yelena Gorlin, Zhebo Chen, and Thomas F. Jaramillo*

Department of Chemical Engineering, Stanford University, Stanford, California 94305-5025, United States

Supporting Information

ABSTRACT: Improving both the activity and the stability of the cathode catalyst in platinum-based polymer electrolyte fuel cells is a key technical challenge. Here, we synthesize a high surface area meso-structured Pt thin film that exhibits higher specific activity for the oxygen reduction reaction (ORR) than commercial carbon-supported Pt nanoparticles (Pt/C). An accelerated stability test demonstrates that the meso-structured Pt thin film also displays significantly enhanced stability as compared to the commercial Pt/C catalyst. Our study reveals the origin of the high turnover frequency (TOF), and excellent durability is attributed to the meso-structure, which yields a morphology with fewer undercoordinated Pt sites than Pt/C nanoparticles, a key difference with substantial impact to the surface chemistry. The improved catalyst activity and stability could enable the development of a high-performance gas diffusion electrode that is resistant to corrosion even under the harsh conditions of start-up, shut-down, and/or hydrogen starvation.

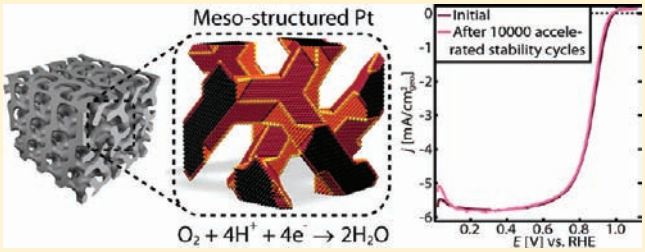

INTRODUCTION

Fuel cell technology is widely believed to play a key role in the next generation of environmentally friendly energy solutions. If powered by fuels (e.g., hydrogen, methanol, etc.) obtained from sustainable energy sources such as wind or solar energy, near-zero emissions of greenhouse gases can be achieved.[1] Over the past decade, there has been significant progress toward meeting the performance and cost targets required for commercialization of proton exchange membrane fuel cells (PEMFCs).[2] One major technical challenge in PEMFC technology is the development of improved cathode catalysts, which drive the oxygen reduction reaction (ORR): $O_2 + 4H^+ + 4e^- \rightarrow 2H_2O$.[2,3] The current industry standard for PEMFC cathodes is a catalyst comprised of Pt nanoparticles supported onto high surface area carbon (Pt/C).[3] Pt/C catalysts have a surface area of 30−90 m^2/g_{Pt}, which results both in high specific activity of approximately 200 $\mu A/cm^2_{Pt}$ and a high mass activity of 0.1−0.3 A/mg_{Pt} at 0.9 V.[3−5] Further improvements in specific and mass activities have been achieved through development of bi- or multimetallic Pt alloys,[6−8] core−shell particles,[9] and introduction of ionic liquids.[10] While improvement of the catalytic activity of the four-electron ORR remains a vital challenge, improving the stability is another key step toward broader PEMFC commercialization. Understanding the mechanisms by which nanoparticulate Pt/C catalysts lose activity over time is paramount to designing a catalyst that can mitigate those undesired processes.

The instability of Pt/C catalysts is ultimately derived from a loss in electrochemical surface area (ECSA) during PEMFC operation conditions.[11] The loss in ECSA can be gradual or sudden.[12] There are three major proposed mechanisms of gradual ECSA loss in Pt/C: (1) Pt sintering by means of particle migration and agglomeration,[13] (2) carbon corrosion, which leads to the detachment of whole Pt particles,[13,14] and (3) dissolution of Pt, which results in Ostwald ripening of nanoparticles as well as the precipitation of Pt in the ionic membrane.[11,15,16] Sudden ECSA loss occurs during the particularly harsh conditions of start-up, shut-down, or hydrogen starvation, and results in quick collapse of carbon support.[12] The ECSA loss contributes to a decrease in the ORR activity and thus a decrease in the overall fuel cell performance. Although efforts to improve the durability of ORR catalysts have not received the same attention as efforts to improve ORR activity, greater research emphasis has been placed on stabilizing Pt catalysts in recent years.[17] Common strategies to improve durability of the Pt/C ORR catalysts include preparation of alloys consisting of Pt and other transition metals,[6,7] synthesis of core−shell type catalysts,[9,18] decoration of Pt nanoparticles with gold clusters,[19] replacement of carbon support with a conductive metal oxide,[20,21] and preparation of unsupported Pt catalysts.[22,23] Approaches to mitigate structural degradation of the carbon support include graphitization of the carbon,[24] addition of an oxygen evolution reaction catalyst to the cathode,[25] and development of an anode that does not catalyze ORR while maintaining high hydrogen oxidation reaction activity.[26]

In this Article, we describe our efforts to improve upon platinum's activity and stability for ORR catalysis by directing the catalyst morphology at the nanoscale. It is well-known that

Received: December 23, 2011
Published: April 13, 2012

   dx.doi.org/10.1021/ja2120162 | J. Am. Chem. Soc. 2012, 134, 7758−7765

flat Pt surfaces exhibit excellent stability and high per-site specific activity, as found for bulk Pt samples as well as for dense films.[3,27,28] However, Pt utilization in these morphologies is generally low, leading to lower mass-specific activities than those observed for Pt/C nanoparticles.[3,28] In our work, we aim to direct the nanostructure of a Pt ORR catalyst such that it exhibits high surface area akin to Pt/C nanoparticles, yet with a surface structure that exhibits excellent stability and per-site activity similar to the properties of bulk Pt.

In pursuit of this goal, we target mesoporous thin films, defined by IUPAC as having pores in the size range of 2−50 nm. Meso-structured materials can exhibit high surface areas[29,30] similar to those observed for supported nanoparticles (30−90 m^2/g_{Pt}),[3] but offer numerous advantages as compared to the morphology of supported nanoparticles. A mesoporous thin film is one contiguous material that is effectively presintered, thus minimizing loss of ECSA due to an agglomeration pathway. It is anchored to the integrated structure at numerous interfacial sites (orders of magnitude more sites than those of a supported nanoparticle), and active sites will likely retain electrical contact with the integrated structure even if some corrosion occurs due to an extensive network of connections within the film itself. In fact, as a mesoporous thin film has inherently high surface area, such films eliminate the need for high surface area carbon supports, which can degrade quickly under certain operating conditions.[12] Omitting the carbon support from the catalyst layer may further reduce the thickness of the catalyst layer and reduce the interfacial resistance in a practical device because the catalyst layer (only mesoporous Pt, no carbon) would be in direct contact with the gas diffusion layer (GDL). Mesoporous structures also exhibit different types of surface sites than nanoparticles and potentially have a smaller fraction of undercoordinated surface atoms, which are known to be the most prone to the dissolution and detachment processes involved in Ostwald ripening.[18,31] Undercoordinated surface Pt atoms are also substantially less active than the more fully coordinated surface atoms on terrace sites.[32−34] Hence, meso-structured Pt films offer advantages over carbon supported Pt nanoparticles when considering all proposed mechanisms of ECSA loss and per-site activity and are excellent candidates for durable and active ORR catalysts. Mesoporous Pt structures have previously been synthesized, often using dealloying techniques.[35] However, to maximize control of pore size and surface structure, we focused our attention on ordered mesoporous morphologies.

A wide range of ordered mesoporous morphologies have been synthesized in the past two decades, many of which have been fabricated as metal oxides, metals, nitrides, and chalcogenides, among other materials.[29,30] To investigate the stability and activity properties of meso-structured Pt films for the ORR, we chose to pursue an extended 3D mesoporous Pt network structure with a double gyroid (DG) morphology, illustrated in Figure 1.

This particular meso-structure exhibits a diffusivity that is higher by an order of magnitude as compared to other mesoporous structures,[36] which we presume will allow facile transport of reactants (O_2 and H^+) and products (H_2O) through the structure. Our studies of ORR catalysis on Pt DG thin films show that this meso-structure is in fact highly active and significantly more stable than commercial Pt/C nanoparticle catalysts, a crucial advancement in ORR catalysis that reveals the potential for meso-structured thin films in accelerating the development and commercialization of PEMFC technology.

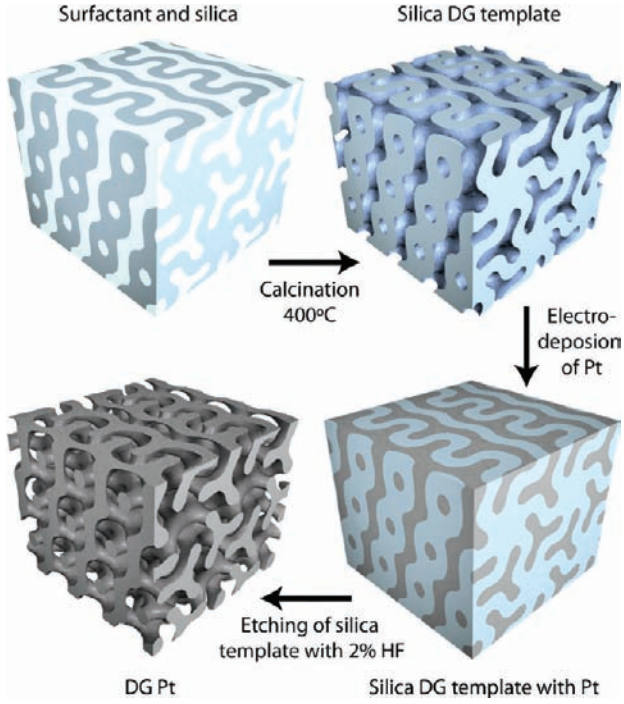

Figure 1. Synthesis procedure and structural model for mesoporous double gyroid (DG) platinum.

EXPERIMENTAL SECTION

The DG Pt structure was synthesized by electrodeposition of Pt into a mesoporous silica film that served as a template atop a glassy carbon (GC) disk (see Figure 1 and the Supporting Information for details). In short, the silica DG template was prepared using an EO_{19}−PO_{43}−EO_{19} surfactant (Pluronic P84, BASF) following the procedure developed by Tate et al.[37] Tetraethyl orthosilicate (TEOS) was prehydrolyzed by mixing with an aqueous solution of HCl and ethanol. The EO_{19}−PO_{43}−EO_{19} surfactant in ethanol was added to the mixture to form the coating solution. Films were dip-coated onto polished GC substrates and dried at a controlled relative humidity of ∼50%, which enabled evaporation-induced self-assembly of the surfactant into the DG structure. After evaporation was complete, the films were calcined in air at 400 °C for 4 h. The calcined silica templates were examined by low angle XRD and TEM to ensure that they exhibited the DG structure (see Figures S1 and S2 in the Supporting Information). Following calcination, Pt was deposited into the template by means of pulsed electrodeposition from an aqueous solution of 0.005 M H_2PtCl_6 in 0.1 M NaCl (see the Supporting Information for details). Last, the silica template was removed by etching with a 2 wt % HF (aq) solution for 30 min, leaving a bicontinuous inverse double gyroid Pt network.

RESULTS AND DISCUSSION

Figure 2a shows an SEM image of the mesoporous Pt DG structure after the silica DG template was removed. The electrodeposited platinum fills the 3D bicontinuous network pore structure of the silica DG template, and thus represents the negative of the silica morphology. The resulting Pt structure is stable after removal of the silica and maintains the interlocked, twisted network structure, as evidenced in the SEM image even though the mesopores are at the limit of the instrument resolution. We note that the Pt DG thin film covers most, but not quite all, of the 5 mm diameter GC disk. This is

dx.doi.org/10.1021/ja2120162 | J. Am. Chem. Soc. 2012, 134, 7758−7765

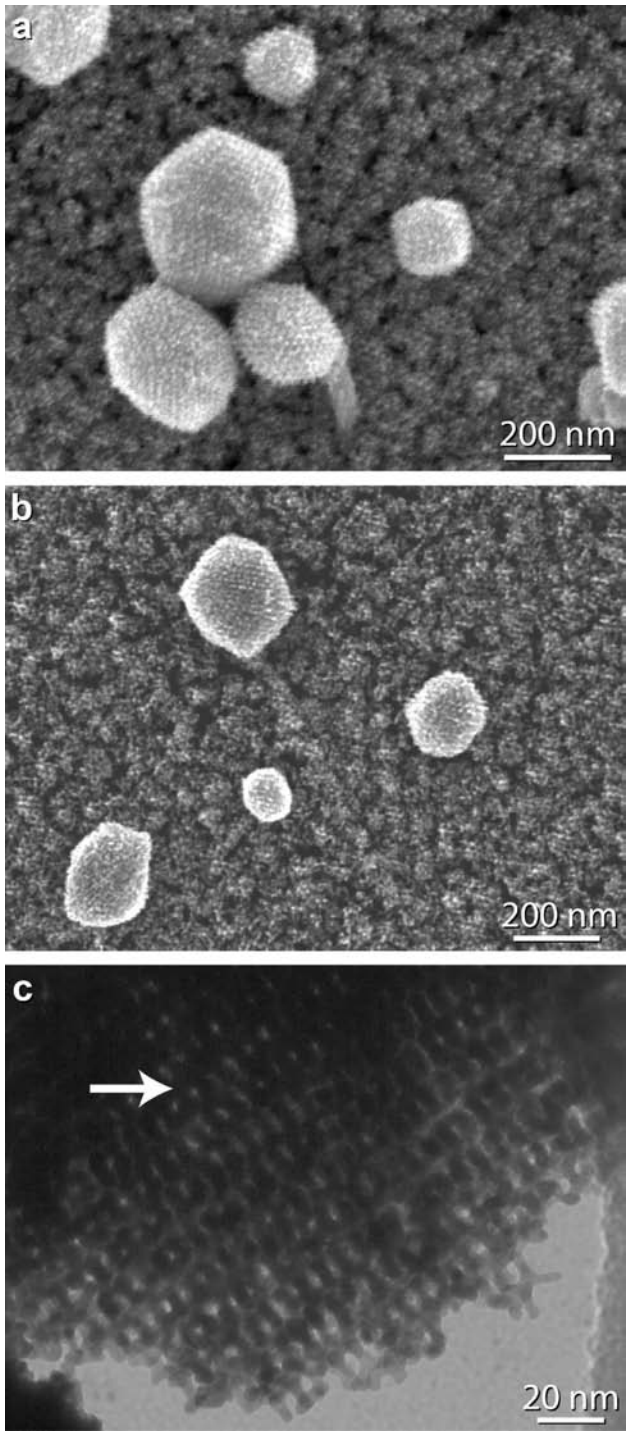

Figure 2. SEM and TEM images of DG Pt. (a and b) SEM images of the DG Pt structure before and after 10 000 accelerated stability test cycles, respectively. (c) TEM image of the DG Pt structure. The elongated hexagonal pattern, indicated by the white arrow, is indicative of the [311] projection of the DG structure.

due to an unavoidable contraction of the silica template, which exposed the bare GC surface at the outer edge where a more dense, non-DG Pt film was deposited (see Figure S4 in the Supporting Information).

On top of the Pt DG film, one can clearly observe faceted particles of approximately 50−300 nm in diameter. These particles are also Pt DG (see SEM images in Figure S3 in the Supporting Information), and grow as an unintended consequence of nonuniform rates of Pt electrodeposition, faster in certain locations on the sample, presumably due to inhomogeneities in the surface chemistry of the carbon substrate. This effect has also been observed with the first reports of the DG Pt morphology synthesized onto fluorine-doped SnO_2 (FTO) supports.[38] The mounds typically grow to have a hexagonal shape as expected from the fcc crystal structure of Pt observed by X-ray diffraction (XRD) (see Figure S1b in the Supporting Information). The TEM image in Figure 2c shows a higher magnification image of the Pt DG mesoporous structure and illustrates the high porosity of these thin films. The average pore-to-pore distance is 6.7 nm, and the pore diameter is 3−4 nm, resulting in a structure with a surface area of 56 m^2/g_{Pt} (see the Supporting Information). The elongated hexagonal pattern as indicated by the white arrow is indicative of the [311] projection of the DG structure.[38] SEM and TEM images thus confirm that we have a highly porous, meso-structured Pt thin film catalyst.

Catalytic activities for the ORR of the as-prepared DG Pt and, for comparison, commercial Pt/C nanoparticles are shown in Figure 3a as linear sweeps in an anodic direction. These measurements were obtained in a rotating disk electrode configuration (RDE), O_2-saturated 0.1 M $HClO_4$ (aq) electrolyte at 23 °C, from 0.02 to 1.12 V versus the reversible hydrogen electrode (RHE) at 5 mV/s and 1600 rpm. The catalyst dispersions of commercial Pt/C nanoparticles (20 wt % Pt on Vulcan XC-72, ETEK, metal concentration of 21 $\mu g/cm^2$) were prepared using standard procedures for fuel cell catalyst testing (see the Supporting Information).[3] The polarization curves for the ORR indicate a positive shift of 30 mV in the half-wave potential ($E_{1/2}$) measured at $j = -3$ mA cm^{-2} and a higher diffusion limited current for DG Pt relative to Pt/C. While these metrics indicate improved activity for DG Pt on geometric basis, the half-wave potential is influenced greatly by Pt loading, and deviations in the diffusion limited current from the theoretical limiting current of −6.0 mA/cm^2 are dependent on film quality.[39,40] Thus, a better approach to compare the ORR kinetics of the two catalysts is to extract the kinetic current from the polarization curves, normalized to the catalytically active surface area. The measured current in the polarization curves is governed by two main contributing factors: an intrinsic kinetic current from O_2 reduction on the surface of the catalyst and a diffusion-limited current. The kinetic current can be calculated using the following equation:

$$\frac{1}{i} = \frac{1}{j_k A_{real}} + \frac{1}{j_d A_{geo}}$$

where A_{real} is the catalytically active surface area (unit: cm^2_{Pt}) approximated by ECSA found from hydrogen underpotential deposition (HUPD), A_{geo} is the geometric area of the disk (0.196 cm^2), and j_k and j_d are the kinetic and diffusion-limited current densities, respectively. The kinetic current densities are displayed as Tafel plots in Figure 3b. The intrinsic kinetic current density at 0.9 V vs RHE is a standard metric for evaluating the specific activities of ORR catalysts.[3] Our measurements on ETEK Pt nanoparticles yielded a specific activity of 180 $\mu A/cm^2_{Pt}$ and a mass-specific activity of 0.09 A/mg_{Pt}, in excellent agreement with previously reported values for ETEK Pt/C measured at the same conditions (O_2-saturated 0.1 M $HClO_4$ (aq), 23 °C, sweep rate 5 mV/s, 1600 rpm).[41,42] We note that higher activity has been reported for both ETEK Pt/C (e.g., specific activity of 261 $\mu A/cm^2_{Pt}$ and mass-specific activity

dx.doi.org/10.1021/ja2120162 | J. Am. Chem. Soc. 2012, 134, 7758−7765

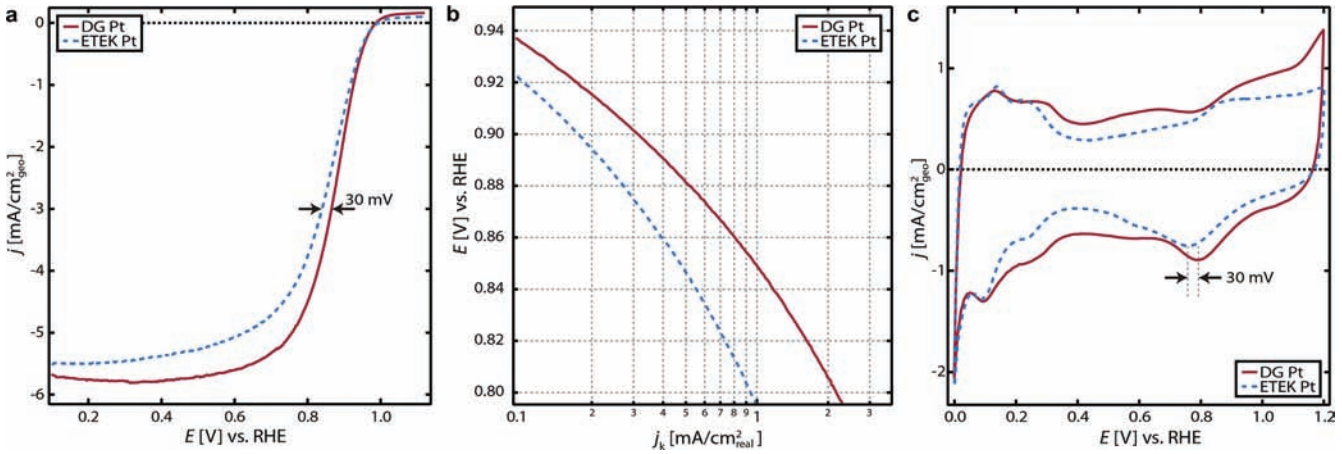

Figure 3. Comparison of the electrocatalytic properties of DG Pt and Pt/C nanoparticles. (a) ORR polarization curves for DG Pt and ETEK Pt/C, respectively. Conditions: O_2-saturated 0.1 M $HClO_4$ (aq), 23 °C, sweep rate 5 mV/s, 1600 rpm. (b) Tafel plot of the kinetic current density from O_2 reduction. (c) Base cyclic voltammograms (CV) of Pt/C (20 wt % Pt on Vulcan XC-72, ETEK) and DG Pt, respectively. Conditions: N_2-purged 0.1 M $HClO_4$ (aq), 23 °C, sweep rate 50 mV/s.

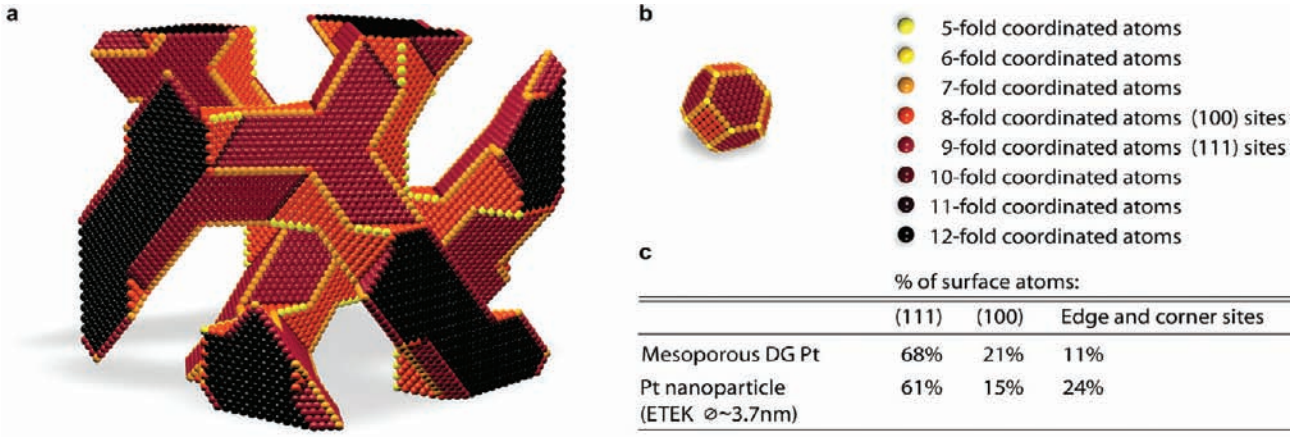

Figure 4. Atomic-scale models of (a) mesoporous DG Pt and (b) Pt nanoparticle with 3.7 nm diameter. The atoms have been colored according to the coordination number; brighter colors indicate atoms with a higher degree of undercoordination. (c) The table shows the distribution of surface atoms in the models shown in (a) and (b), respectively. The mesoporous DG Pt structure contains a smaller fraction of undercoordinated edge and corner sites as compared to Pt nanoparticles.

of 0.16 A/mg_{Pt})[4] and TKK (Tanaka Kikinzoku Kogyo, Tokyo) Pt/C nanoparticles (e.g., specific activity of 360 $\mu A/cm^2_{Pt}$ and mass-specific activity of 0.33 A/mg_{Pt}).[5] The mesoporous DG Pt catalyst achieves a specific activity of 310 $\mu A/cm^2_{Pt}$, which is on par with the very best Pt/C catalysts. To determine mass-specific activity of the DG Pt catalyst, the total Pt mass on the GC disk was measured by an inductively coupled plasma optical emission spectrometer (ICP-OES, Thermo Scientific ICAP 6300). A measured loading of 14 μg yields an overall electrode mass-specific activity of 0.04 A/mg_{Pt}. However, we believe the value of 0.04 A/mg_{Pt} represents a lower-bound measurement for DG Pt because the electrode consisted of both a DG Pt phase as well as a denser, non-DG phase unavoidably produced along the rim of the GC disk (see SEM images in Figure S4 in the Supporting Information). Samples with larger rims of non-DG Pt (and hence lower amount of DG Pt) showed lower activity and lower Pt surface area, from which we infer that both activity and Pt surface area are controlled by the DG Pt phase. A calculation of the mass of the DG Pt phase based on the Pt surface area as measured from HUPD and 3D models of the DG structure indicates that the mass of the DG Pt phase is actually 2.9 μg. From this value, we estimate the upper-bound mass-specific activity (assuming negligible current contribution from the non-DG Pt phase) of the DG Pt phase to be 0.17 A/mg_{Pt} (see the Supporting Information for details on the calculations). Thus, we estimate that the DG structured Pt catalyst exhibits a mass-specific activity within a factor of 2 of the very best Pt/C catalysts. Additionally, the DG Pt catalyst exhibits no apparent transport limitations.

To understand why the meso-structured Pt film exhibits a greater per site activity than the supported nanoparticles, we focused our attention to the surface structure of the two nanomaterials. The two morphologies have relatively similar surface areas, approximately 50−60 m^2/g (see the Supporting Information), but are expected to have different distributions of surface sites. This difference will affect the specific activity, because the Pt surface structure has a significant impact on ORR catalysis. Undercoordinated Pt atoms, such as those that are found on step sites, corner sites, and edge sites, etc., are expected to be less active for the ORR than atoms on the flat planes[32−34] because undercoordinated Pt atoms will form a much stronger bond to key reactive intermediates on the surface such as O_{ads} and OH_{ads}. This is an undesirable effect for Pt-based catalysts whose turnover is impeded by binding

dx.doi.org/10.1021/ja2120162 | J. Am. Chem. Soc. 2012, 134, 7758−7765

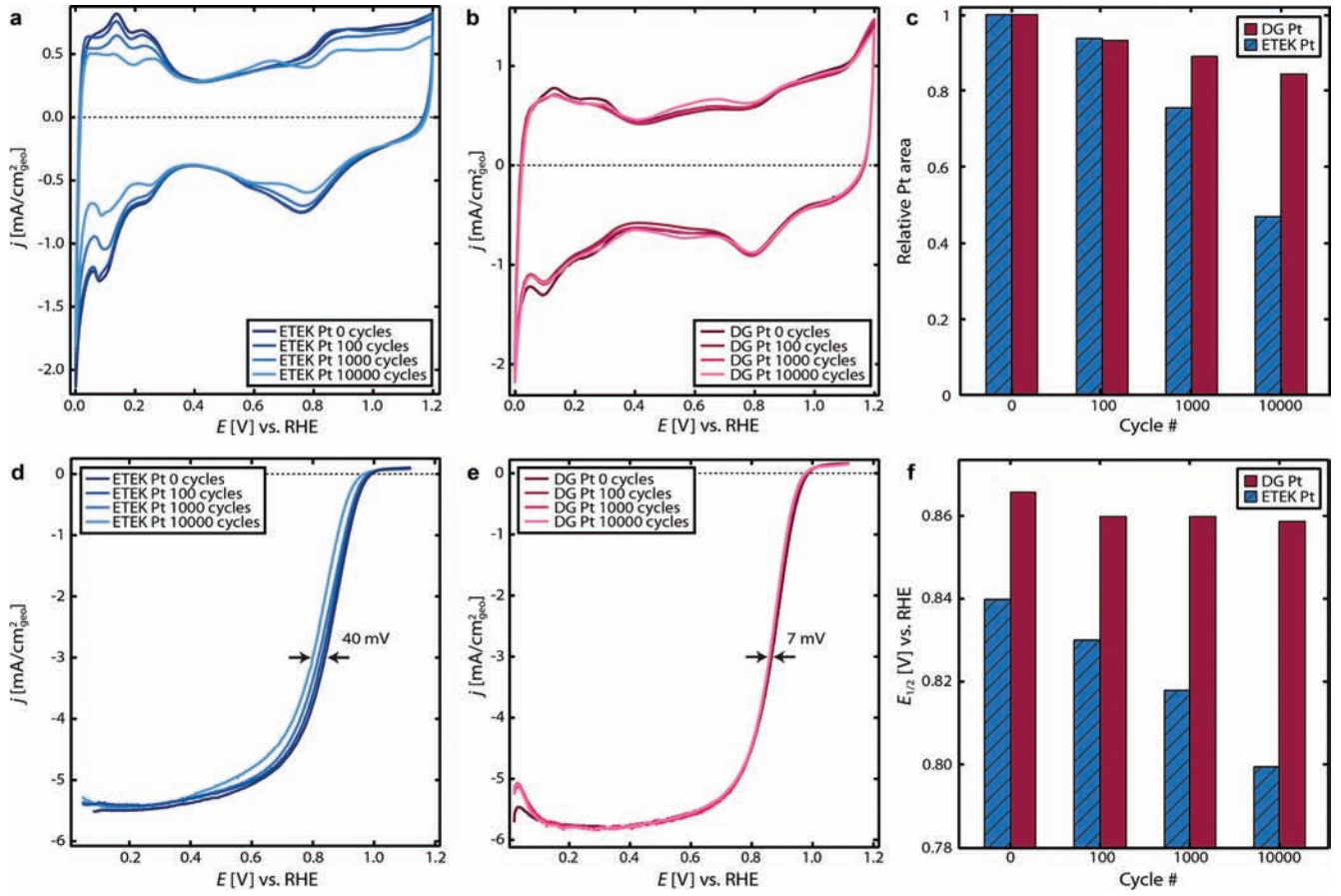

Figure 5. Comparison of the stability of DG Pt and Pt/C nanoparticles. (a and b) Initial and post potential cycling CV curves for ETEK Pt/C nanoparticles and DG Pt, respectively. Conditions: N_2-purged 0.1 M $HClO_4$ (aq), 23 °C, sweep rate 50 mV/s. (c) Relative Pt area as measured by HUPD as a function of accelerated stability test cycles. (d and e) Initial and post potential cycling ORR polarization curves for ETEK Pt/C nanoparticles and DG Pt, respectively. Conditions: O_2-saturated 0.1 M $HClO_4$ (aq), 23 °C, sweep rate 5 mV/s, 1600 rpm. (f) Half-wave potentials ($E_{1/2}$) measured at $j = -3$ mA cm^{-2} as a function of accelerated stability test cycles.

reaction intermediates too strongly.[33,43,44] Pt nanoparticles, which are approximately spherical or hemispherical in shape with purely convex features, have a significant radius of curvature that leads to a large fraction of undercoordinated sites on the surface. Although meso-structured materials have feature sizes on the nanoscale as well, the contiguous nature of the material and its composition of both convex and concave features could lead to a different atomic-scale surface structure, potentially one with a smaller fraction of undercoordinated sites.

To probe the surface structure of these catalysts, base cyclic voltammograms (CVs) in a N_2-saturated environment were employed to measure the adsorption strength of O_{ads} and OH_{ads}. The initial base CVs of Pt/C and DG Pt are shown in Figure 3c (N_2-saturated 0.1 M $HClO_4$ (aq) electrolyte from 0.0 to 1.2 V vs RHE at 50 mV/s and 0 rpm). The region above ca. +0.6 V is dominated by the reversible adsorption/desorption of OH_{ads}. Careful inspection of the CVs reveals that the OH_{ads} adsorption/desorption peaks for DG Pt are positively shifted about 30 mV relative to Pt/C. This indicates that the surface sites on DG Pt do not bind O_{ads} and OH_{ads} as strongly as the surface sites on nanoparticulate Pt/C. Mayrhofer et al. previously investigated the size-dependent electrocatalytic properties of Pt nanoparticles.[45] They found a similar positive shift of OH_{ads} adsorption/desorption peaks with increasing particle size, as one might expect with flatter surfaces and increasing average atomic coordination number. Comparison of the OH_{ads} adsorption/desorption peak positions in the base CV of the DG Pt with the peak positions in base CVs of the different sized nanoparticles studied by Mayrhofer et al.[45] reveals that, despite having a high surface area on par with small nanoparticles, the surface structure of DG Pt is more comparable to large particles than to small nanoparticles, as evidenced by similarities in binding OH_{ads}.

To understand the origin of this experimental observation, we constructed atomic-scale models of 3.7 nm diameter Pt nanoparticles as well as the inverse DG Pt morphology as shown in Figure 4. The model of the nanoparticle is the standard cuboctahedron, which is widely accepted in the literature as a reasonable approximation to commercial 3−5 nm supported Pt nanoparticles,[46] and 3.7 nm was found by Schmidt et al. to be the mean size of pretreated 20 wt % Pt on Vulcan XC-72, ETEK nanoparticles.[47] This nanoparticle model exhibits a distribution of surface atoms of approximately 61% (111) facets, 15% (100) facets, and 24% edge and corner sites. The atomic-scale model of the inverse DG structure, on the other hand, reveals a different distribution of surface atoms, consisting of 68% (111) facets, 21% (100) facets, and 11% edge and corner sites. These idealized models are meant to reflect the wide range of possible structures that constitute the true catalyst surface in either case. The models are consistent with the experimental observations and qualitatively explain the

dx.doi.org/10.1021/ja2120162 | J. Am. Chem. Soc. 2012, 134, 7758−7765

origin of the improved per site activity of DG Pt over Pt/C: the DG Pt structure exhibits a smaller fraction of undercoordinated surface sites as compared to Pt/C, despite the fact that both possess similarly high surface areas. We are the first to establish that one can develop an unsupported Pt catalyst with as high a surface area as Pt/C nanoparticles, but with an improved per site activity.

As stated earlier, stability is a critical concern for ORR catalysts. To study the stability of DG Pt, we adopted a slightly modified version of the DOE protocol[48] for ORR catalyst accelerated durability tests, which aim to simulate the working conditions of fuel cells. The accelerated stability tests were performed by continuously cycling the potential between 0.6 and 1.1 V vs RHE at a sweep rate of 50 mV/s in an O_2-saturated 0.1 M $HClO_4$ (aq) solution at 23 °C (see the Supporting Information for more details). Potential cycling between 0.6 and 1.1 V causes alternating surface oxidation/reduction of the Pt, which is particularly vigorous due to the dynamic nature of the surface changes. The catalytic ORR activity and the ECSA of DG Pt catalyst were evaluated initially and immediately following 100, 1000, and 10 000 accelerated stability test cycles, using the conditions described above. Before every ORR activity and ECSA measurement, the solution was replaced with fresh electrolyte, and the sample was cleaned by electrochemical cycling in N_2-saturated electrolyte from −0.06 to 1.17 V vs RHE at 500 mV/s and 0 rpm to maximize ORR activity and ECSA. The cleaning cycles were continued until stable CVs were obtained (50−300 cycles).

The cyclic voltammograms displaying the hydrogen underpotential deposition (HUPD) region are shown in Figure 5a and b for Pt/C nanoparticles and DG Pt, respectively. The ECSA was determined by integrating the charge from 0.05 to 0.4 V vs RHE after subtraction of the double layer capacitance and assuming a charge density of 210 $\mu C/cm^2_{Pt}$ for polycrystalline Pt.[3,47] The ECSA data are summarized in Table 1.

Table 1. Area, Relative Area, and Half-Wave Potential ($E_{1/2}$) for DG Pt and ETEK Pt/C Nanoparticles

	double gyroid Pt			ETEK Pt/C		
cycle no.	Pt area [cm^2/cm^2_{geo}]	relative Pt area	$E_{1/2}$ (j = −3 mA cm^{-2}) [V] vs RHE	Pt area [cm^2/cm^2_{geo}]	relative Pt area	$E_{1/2}$ (j = −3 mA cm^{-2}) [V] vs RHE
0	8.33	1.00	0.866	10.78	1.00	0.840
100	7.79	0.94	0.860	10.13	0.94	0.830
1000	7.40	0.88	0.860	8.14	0.75	0.818
10 000	7.02	0.84	0.859	5.07	0.47	0.800

After the first 100 cycles, the Pt/C nanoparticles experience an initial loss of ∼6%, and continue to lose ECSA with additional potential cycling as previously reported in the literature.[14,19,49] After 10 000 cycles, the ECSA is below 50% of its initial value; see Table 1 and Figure 5c. Furthermore, the Pt/C nanoparticles show a degradation in the half-wave potential with increasing potential cycling as observed in Figure 5d, which displays the initial and post potential cycling catalytic activities for ORR as linear sweeps in the anodic direction. After 10 000 cycles, the half-wave potential decreased by 40 mV; see Table 1 and Figure 5f.

The accelerated durability tests reveal that DG Pt is significantly more stable than Pt/C. After the initial 100 cycles, DG Pt experiences a loss of ∼6% similar to Pt/C. However, with continued potential cycling, the loss of ECSA in the DG Pt is much slower than that with the Pt/C nanoparticles. Even after 10 000 cycles, DG Pt maintains over 80% of the initial ECSA (see Table 1 and Figure 5c). Moreover, the initial and post potential cycling catalytic ORR activities shown in Figure 5e reveal that after 10 000 cycles, DG Pt shows a degradation in the half-wave potential of only 7 mV. This minimal change in the half-wave potential of Pt DG catalyst further illustrates the increased stability of DG Pt over Pt/C nanoparticles.

To evaluate the physical condition of the DG Pt after the accelerated stability tests, we performed SEM imaging. Figure 2b shows a SEM image of the DG Pt sample after 10 000 cycles with no visible degradation. Even the faceted DG Pt particles are still present, which indicates a strong metallic bond between the particulates and the uniform DG Pt thin film underneath. We suspect that the small loss in ESCA for the Pt DG catalyst likely arises from dissolution of Pt atoms from undercoordinated surface sites and possibly from the detachment of some of the Pt DG particles that rest atop the thin film. Overall, the DG Pt meso-structure remains intact even after intensive accelerated stability tests, and this superior stability over Pt/C nanoparticles shows the promise of controlling the morphology of Pt and Pt-based ORR catalyst materials at the nanoscale, particularly in the form of mesoporous thin films.

CONCLUSION

To facilitate the kinetics of ORR catalysis and to simultaneously counteract mechanisms for catalyst degradation, we directed the morphology of Pt to develop a catalyst nanostructure with high specific activity and superior durability as compared to commercial Pt/C nanoparticulate catalysts. The DG meso-structure exhibits excellent specific activity due to a surface structure with a lower fraction of undercoordinated Pt atoms. In addition, the lower and upper bound mass activities for the DG Pt are within the same range of values found for various loadings of ETEK Pt/C. The thin film nature of our catalyst begets a significantly improved stability for several reasons. First, the contiguous nature of the meso-structured network limits the pathways for Ostwald ripening, Pt migration, and agglomeration, processes that adversely affect the stability of nanoparticulate catalysts.[11,13,16] Second, it mitigates carbon corrosion issues that lead to catalyst detachment and a loss of ECSA in Pt/C catalysts.[13,14] A recent review concludes that, while advanced carbon supports (nanofibers, hierarchical carbon, mesoporous carbon, etc.) and/or functionalizing carbon surface may increase the stability relative to traditional carbon supports, it is unlikely that a carbon-only support will lead to simultaneous high activity, high stability PEMFC cathode electrocatalysts.[50] Ultimately, the DG Pt structure could eliminate the need for carbon support altogether; because the high surface area of the meso-structured Pt film is inherent to the film and not to the support, high surface area carbon is not needed to achieve high mass activity or electrode porosity. This is important for start-up and shut-down conditions during which carbon support has been shown to corrode and suffer structural collapse.[12] The possibility to omit high surface area carbon support also opens opportunity for high temperature PEMFCs, which can achieve more facile electrochemical cathode kinetics and improved tolerance to contaminants, such as CO, in the fuel,[51] but suffer from increased corrosion of the carbon support.[51,52] Third, platinum dissolution is also expected to be mitigated in the meso-structure versus

dx.doi.org/10.1021/ja2120162 | J. Am. Chem. Soc. 2012, 134, 7758−7765

nanoparticulate catalysts as the interlocked continuous DG network exhibits a smaller fraction of undercoordinated Pt atoms at the surface and has a surface structure that is more comparable to large nanoparticles than to small nanoparticles. This notion is supported by recent work from Holby and co-workers in which they showed that the use of larger nanoparticles instead of 2−3 nm nanoparticles commonly used in PEMFC cathodes would significantly decrease Pt dissolution.[53] The high stability, high specific activity, and good mass-transport properties of DG Pt catalyst render it a promising cathode catalyst for PEMFCs.

The future is promising for meso-structured thin film ORR catalysts. A large number of viable mesoporous morphologies are worthy of exploration as the DG morphology is one of many possibilities; we aim to continue our investigations into other morphologies as we concurrently develop a means to integrate this catalyst structure into a membrane electrode assembly (MEA). One means to do so might involve self-assembled crystalline whiskers, which have recently shown great promise as a support for Pt and Pt-alloy catalysts. Nanostructured Pt thin films employing these whiskers (Pt/NSTF) show a very high specific activity of 1.65 mA/cm^2_{Pt} (O_2-saturated 0.1 M $HClO_4$ (aq), 20 °C, sweep rate 20 mV/s, 1600 rpm)[54] and good stability, maintaining 67% of initial ECSA after 9000 cycles in an accelerated MEA test.[55] The stable performance was attributed to the thin film nature of Pt thin film as opposed to individual nanoparticles, possessing advantages similar to those discussed in the present work on DG Pt. However, the main drawback for Pt/NSTF is the dense nature of the Pt thin film, which results in lower mass specific activity (0.12 A/mg_{Pt}).[54] In this regard, it would be intriguing to substitute the dense Pt thin film with a coating of DG Pt on the whiskers, which would increase the surface to volume fraction of Pt along with the specific mass activity, while still maintaining excellent stability as shown in this work.

It would also be interesting to examine the activity and durability of mesoporous platinum-based alloys because alloys such as Pt_3Ni[6,56] and more recently Pt_3Y[7] have been shown to be the most active catalysts for oxygen reduction reaction with an order of magnitude higher activity than pure Pt catalysts. Furthermore, the high porosity of the DG structure makes it a promising candidate for impregnation with high-oxygen-solubility ionic liquids, which recently have been shown to improve ORR catalysis.[10] On a final note, the concept of using meso-structured DG materials as active and durable catalysts is not limited to the ORR. There are a number of other electrochemical reactions where dissolution, sintering, or detachment of the electrocatalyst is problematic; morphological control of the catalyst structure, as shown in this work, could be of general use in developing improved catalyst materials.

■ ASSOCIATED CONTENT

Supporting Information

Detailed information on the synthesis procedure and experimental characterizations, including XRD spectra of DG silica templates and DG Pt and TEM image of the silica DG template. Calculations of mass-specific area and activity. This material is available free of charge via the Internet at http://pubs.acs.org.

■ AUTHOR INFORMATION

Corresponding Author

jaramillo@stanford.edu

Notes

The authors declare no competing financial interest.

■ ACKNOWLEDGMENTS

This work was supported as part of the Center on Nanostructuring for Efficient Energy Conversion (CNEEC) at Stanford University, an Energy Frontier Research Center funded by the U.S. Department of Energy, Office of Science, and Office of Basic Energy Sciences under Award Number DE-SC0001060. We thank BASF for generously providing the surfactant Pluronic P84. Mr. Benjamin N. Reinecke is acknowledged for TEM imaging. J.K. gratefully acknowledges the Villum Kann Rasmussen Foundation for a postdoctoral fellowship.

■ REFERENCES

(1) Bak, T.; Nowotny, J.; Rekas, M.; Sorrell, C. C. *Int. J. Hydrogen Energy* **2002**, *27*, 991.
(2) Vielstich, W.; Gasteiger, H. A.; Lamm, A.; Yokokawa, H. *Handbook of Fuel Cells: Fundamentals, Technology, and Applications*; John Wiley & Sons Ltd.: New York, 2009.
(3) Gasteiger, H. A.; Kocha, S. S.; Sompalli, B.; Wagner, F. T. *Appl. Catal., B* **2005**, *56*, 9.
(4) Garsany, Y.; Baturina, O. A.; Swider-Lyons, K. E.; Kocha, S. S. *Anal. Chem.* **2010**, *82*, 6321.
(5) Kim, J.; Lee, S. W.; Carlton, C.; Shao-Horn, Y. *J. Phys. Chem. Lett.* **2011**, *2*, 1332.
(6) Stamenkovic, V. R.; Fowler, B.; Mun, B. S.; Wang, G.; Ross, P. N.; Lucas, C. A.; Marković, N. M. *Science* **2007**, *315*, 493.
(7) Greeley, J.; Stephens, I. E. L.; Bondarenko, A. S.; Johansson, T. P.; Hansen, H. A.; Jaramillo, T. F.; Rossmeisl, J.; Chorkendorff, I.; Nørskov, J. K. *Nat. Chem.* **2009**, *1*, 552.
(8) Lim, B.; Jiang, M. J.; Camargo, P. H. C.; Cho, E. C.; Tao, J.; Lu, X. M.; Zhu, Y. M.; Xia, Y. A. *Science* **2009**, *324*, 1302.
(9) Gong, K. P.; Su, D.; Adzic, R. R. *J. Am. Chem. Soc.* **2010**, *132*, 14364.
(10) Snyder, J.; Fujita, T.; Chen, M. W.; Erlebacher, J. *Nat. Mater.* **2010**, *9*, 904.
(11) Ferreira, P. J.; la O, G. J.; Shao-Horn, Y.; Morgan, D.; Makharia, R.; Kocha, S.; Gasteiger, H. A. *J. Electrochem. Soc.* **2005**, *152*, A2256.
(12) Reiser, C. A.; Bregoli, L.; Patterson, T. W.; Yi, J. S.; Yang, J. D.; Perry, M. L.; Jarvi, T. D. *Electrochem. Solid-State Lett.* **2005**, *8*, A273.
(13) Hartl, K.; Nesselberger, M.; Mayrhofer, K. J. J.; Kunz, S.; Schweinberger, F. F.; Kwon, G.; Hanzlik, M.; Heiz, U.; Arenz, M. *Electrochim. Acta* **2010**, *56*, 810.
(14) Mayrhofer, K. J. J.; Meier, J. C.; Ashton, S. J.; Wiberg, G. K. H.; Kraus, F.; Hanzlik, M.; Arenz, M. *Electrochem. Commun.* **2008**, *10*, 1144.
(15) Perez-Alonso, F. J.; Elkjær, C. F.; Shim, S. S.; Abrams, B. L.; Stephens, I. E. L.; Chorkendorff, I. *J. Power Sources* **2011**, *196*, 6085.
(16) Shao-Horn, Y.; Sheng, W.; Chen, S.; Ferreira, P.; Holby, E.; Morgan, D. *Top. Catal.* **2007**, *46*, 285.
(17) Gasteiger, H. A.; Gu, W.; Litteer, B.; Makharia, R.; Brady, B.; Budnski, M.; Thompson, E.; Wagner, F. T.; Yan, S. G.; Yu, P. T. In *Mini-Micro Fuel Cells: Fundamentals and Applications*; Kakac, S., Pramuanjaroenkij, A., Vasiliev, L., Eds.; Springer, Dordrecht: The Netherlands, 2008; p 225.
(18) Wang, J. X.; Ma, C.; Choi, Y.; Su, D.; Zhu, Y.; Liu, P.; Si, R.; Vukmirovic, M. B.; Zhang, Y.; Adzic, R. R. *J. Am. Chem. Soc.* **2011**, *133*, 13551.
(19) Zhang, J.; Sasaki, K.; Sutter, E.; Adzic, R. R. *Science* **2007**, *315*, 220.
(20) Sasaki, K.; Zhang, L.; Adzic, R. R. *Phys. Chem. Chem. Phys.* **2008**, *10*, 159.
(21) Huang, S.-Y.; Ganesan, P.; Park, S.; Popov, B. N. *J. Am. Chem. Soc.* **2009**, *131*, 13898.
(22) Antolini, E.; Perez, J. *J. Mater. Sci.* **2011**, *46*, 4435.

(23) Wang, H.-H.; Zhou, Z.-Y.; Yuan, Q.; Tian, N.; Sun, S.-G. *Chem. Commun.* **2011**, *47*, 3407.
(24) Yu, P. T.; Gu, W.; Makharia, R.; Wagner, F. T.; Gasteiger, H. A. *ECS Trans.* **2006**, *3*, 797.
(25) Atanasoska, L. L.; Vernstrom, G.; Haugen, G. M.; Atanasoski, R. *ECS Trans.* **2011**, *41*, 785.
(26) Genorio, B.; Subbaraman, R.; Strmcnik, D.; Tripkovic, D.; Stamenkovic, V. R.; Markovic, N. M. *Angew. Chem., Int. Ed.* **2011**, *50*, 5468.
(27) Komanicky, V.; Chang, K. C.; Menzel, A.; Markovic, N. M.; You, H.; Wang, X.; Myers, D. *J. Electrochem. Soc.* **2006**, *153*, B446.
(28) Nesselberger, M.; Ashton, S.; Meier, J. C.; Katsounaros, I.; Mayrhofer, K. J. J.; Arenz, M. *J. Am. Chem. Soc.* **2011**, *133*, 17428.
(29) Wan, Y.; Shi, Y.; Zhao, D. *Chem. Commun.* **2007**, 897.
(30) Sanchez, C.; Boissière, C.; Grosso, D.; Laberty, C.; Nicole, L. *Chem. Mater.* **2008**, *20*, 682.
(31) Rinaldo, S. G.; Stumper, J. R.; Eikerling, M. *J. Phys. Chem. C* **2010**, *114*, 5773.
(32) Kinoshita, K. *J. Electrochem. Soc.* **1990**, *137*, 845.
(33) Greeley, J.; Rossmeisl, J.; Hellman, A.; Nørskov, J. K. *Z. Phys. Chem.* **2007**, *221*, 1209.
(34) Mayrhofer, K. J. J.; Strmcnik, D.; Blizanac, B. B.; Stamenkovic, V.; Arenz, M.; Markovic, N. M. *Electrochim. Acta* **2008**, *53*, 3181.
(35) Ding, Y.; Mathur, A.; Chen, M.; Erlebacher, J. *Angew. Chem., Int. Ed.* **2005**, *44*, 4002.
(36) Wei, T. C.; Hillhouse, H. W. *Langmuir* **2007**, *23*, 5689.
(37) Tate, M. P.; Urade, V. N.; Gaik, S. J.; Muzzillo, C. P.; Hillhouse, H. W. *Langmuir* **2010**, *26*, 4357.
(38) Urade, V. N.; Wei, T. C.; Tate, M. P.; Kowalski, J. D.; Hillhouse, H. W. *Chem. Mater.* **2007**, *19*, 768.
(39) Stamenković, V.; Schmidt, T. J.; Ross, P. N.; Marković, N. M. *J. Electroanal. Chem.* **2003**, *554*−*555*, 191.
(40) Garsany, Y.; Singer, I. L.; Swider-Lyons, K. E. *J. Electroanal. Chem.* **2011**, *662*, 396.
(41) Paulus, U. A.; Wokaun, A.; Scherer, G. G.; Schmidt, T. J.; Stamenkovic, V.; Radmilovic, V.; Markovic, N. M.; Ross, P. N. *J. Phys. Chem. B* **2002**, *106*, 4181.
(42) Schulenburg, H.; Müller, E.; Khelashvili, G.; Roser, T.; Bönnemann, H.; Wokaun, A.; Scherer, G. G. *J. Phys. Chem. C* **2009**, *113*, 4069.
(43) Markovic, N. M.; Ross, P. N. *Surf. Sci. Rep.* **2002**, *45*, 117.
(44) Tritsaris, G.; Greeley, J.; Rossmeisl, J.; Nørskov, J. *Catal. Lett.* **2011**, *141*, 909.
(45) Mayrhofer, K. J. J.; Blizanac, B. B.; Arenz, M.; Stamenkovic, V. R.; Ross, P. N.; Markovic, N. M. *J. Phys. Chem. B* **2005**, *109*, 14433.
(46) Schmidt, T. J.; Paulus, U. A.; Gasteiger, H. A.; Behm, R. J. *J. Electroanal. Chem.* **2001**, *508*, 41.
(47) Schmidt, T. J.; Gasteiger, H. A.; Stab, G. D.; Urban, P. M.; Kolb, D. M.; Behm, R. J. *J. Electrochem. Soc.* **1998**, *145*, 2354.
(48) *Cell Component Accelerated Stress Test Protocols for PEM Fuel Cells*; U.S. Department of Energy: http://www1.eere.energy.gov/hydrogenandfuelcells/pdfs/component_durability_may_2010.pdf, 2010.
(49) Mathias, M. F.; Makharia, R.; Gasteiger, H. A.; Conley, J. J.; Fuller, T. J.; Gittleman, C. J.; Kocha, S. S.; Miller, D. P.; Mittelsteadt, C. K.; Xie, T.; Yan, S. G.; Yu, P. T. *Electrochem. Soc. Interface* **2005**, *14*, 24.
(50) Shrestha, S.; Liu, Y.; Mustain, W. E. *Catal. Rev.* **2011**, *53*, 256.
(51) Zhang, J.; Xie, Z.; Zhang, J.; Tang, Y.; Song, C.; Navessin, T.; Shi, Z.; Song, D.; Wang, H.; Wilkinson, D. P.; Liu, Z.-S.; Holdcroft, S. *J. Power Sources* **2006**, *160*, 872.
(52) Stevens, D. A.; Dahn, J. R. *Carbon* **2005**, *43*, 179.
(53) Holby, E. F.; Sheng, W.; Shao-Horn, Y.; Morgan, D. *Energy Environ. Sci.* **2009**, *2*, 865.
(54) van der Vliet, D.; Wang, C.; Debe, M.; Atanasoski, R.; Markovic, N. M.; Stamenkovic, V. R. *Electrochim. Acta* **2011**, *56*, 8695.
(55) Debe, M. K.; Schmoeckel, A. K.; Vernstrom, G. D.; Atanasoski, R. *J. Power Sources* **2006**, *161*, 1002.
(56) Zhang, J.; Yang, H.; Fang, J.; Zou, S. *Nano Lett.* **2010**, *10*, 638.